



Cite this: *J. Mater. Chem. C*, 2017,
5, 5334

Polypyrrole-interface-functionalized nano-magnetite epoxy nanocomposites as electromagnetic wave absorbers with enhanced flame retardancy†

Jiang Guo,^{ab} Haixiang Song,^b Hu Liu,^b Chunjia Luo,^c Yanrong Ren,^a Tao Ding,^{*a} Mojammel A. Khan,^d David P. Young,^d Xinyu Liu,^e Xin Zhang,^f Jie Kong ^{*c} and Zhanhu Guo ^{*b}

Epoxy nanocomposites reinforced with polypyrrole functionalized nano-magnetite (Fe₃O₄-PPy) showed significantly enhanced electromagnetic wave absorption performance and flame retardancy. The Fe₃O₄-PPy nanocomposites were prepared by the surface initiated polymerization method. The epoxy/(30.0 wt%)Fe₃O₄-PPy nanocomposites possess a minimum reflection loss (RL) value of -35.7 dB, which is much lower than that of either epoxy/(7.5 wt%)PPy nanocomposites with a minimum RL value of -11.0 dB or epoxy/(30.0 wt%)Fe₃O₄ with a minimum RL value of -17.8 dB at the same thickness (1.7 mm). Meanwhile, the bandwidth of epoxy/(30.0 wt%)Fe₃O₄-PPy nanocomposites for RL < -10 dB and RL < -20 dB is 4.0 GHz and 0.8 GHz, respectively. The increased interface area, eddy current loss and anisotropic energy are essentially important to achieve higher reflection loss and broader absorption bandwidth for epoxy/(30.0 wt%)Fe₃O₄-PPy nanocomposites. Moreover, the significantly reduced flammability was observed in the epoxy/(30.0 wt%)Fe₃O₄-PPy nanocomposites compared with pure epoxy. The total heat release of epoxy/(30.0 wt%)Fe₃O₄-PPy nanocomposites decreased from 25.5 kJ g⁻¹ of pure epoxy to just 12.3 kJ g⁻¹. The tensile strength of the epoxy nanocomposites was reported as well. These new nanocomposites with an enhanced electromagnetic wave absorption property and flame retardancy possess great potential for safer electromagnetic wave absorbers in the electronic industry to satisfy stringent industrial standards.

Received 7th April 2017,
Accepted 20th April 2017

DOI: 10.1039/c7tc01502j

rsc.li/materials-c

1. Introduction

Nowadays, due to the rapid development of information technology, electronic devices have been widely used for commercial and military applications.^{1,2} The electromagnetic waves have been deployed in wireless cell phones, local area networks and other communication facilities.³ However, usage of electronic devices usually leads to serious electromagnetic interference

(EMI) problem.⁴ Human beings have paid much attention to this problem because of the harmful effect of electromagnetic radiation.⁵ Therefore, suitable materials that can absorb electromagnetic waves are urgently needed. In recent years, polymer nanocomposites have been widely studied due to their cost-effective processability, light weight, enhanced mechanical properties and unique physicochemical properties.⁶⁻¹⁵ Polymer nanocomposites are one of the best materials for electromagnetic wave absorption in a wide absorption frequency range.¹⁶⁻¹⁸ Epoxy resin, as a typical engineering thermosetting material, has been widely used in the industry for various applications such as coating and adhesives, due to the high Young's modulus, chemical resistance, and good thermal stability.^{7,19-24} In order to widen the application of epoxy resin for EMI shielding application, different nanofillers were added. For example, Liang *et al.* synthesized graphene epoxy nanocomposites with enhanced EMI shielding performance.¹ Kim *et al.* reported nickel coated multi-walled carbon nanotubes epoxy nanocomposites with increased EMI shielding efficiency.²⁵

The electrically conductive polypyrrole (PPy) has been widely studied for various applications such as biosensors, membranes, coating materials, energy storage, photovoltaic cells and EMI

^a College of Chemistry and Chemical Engineering, Henan University, Kaifeng 475004, P. R. China. E-mail: dingtao@henu.edu.cn

^b Integrated Composites Laboratory (ICL), Department of Chemical & Biomolecular Engineering, University of Tennessee, Knoxville, TN, 37996, USA. E-mail: zguo10@utk.edu

^c Shaanxi Key Laboratory of Macromolecular Science and Technology, School of Science, Northwestern Polytechnical University, Xi'an, 710072, P. R. China. E-mail: kongjie@nwpu.edu.cn

^d Department of Physics and Astronomy, Louisiana State University, Baton Rouge, LA 70803, USA

^e Department of Industrial Engineering, Lamar University, Beaumont, TX 77710, USA

^f Physical Sciences Division, Pacific Northwest National Laboratory, Richland, WA 99354, USA

† Electronic supplementary information (ESI) available. See DOI: 10.1039/c7tc01502j

shielding, because of its low cost, easy preparation, high yield and excellent electrical properties.^{26–30} Recently, PPy based nanocomposites for EMI shielding have been reported. For example, Kim *et al.* synthesized PPy–nylon 6 composite fabrics in which the EMI shielding efficiency was dependent on the electrical conductivity and the layer array sequence.³¹ Avlioni *et al.* studied the PPy-coated polyester nonwoven textiles, and these composites with low surface electrical conductivity showed a better EMI shielding efficiency.³² Although PPy has some advantages in EMI shielding application, there are two shortcomings. First, as a non-magnetic material, only the dielectric loss can affect the EMI shielding performance. Second, the dielectric permittivity and magnetic permeability are out of balance for PPy, resulting in a bad impedance matching. In order to overcome these defects, magnetic nanoparticles are needed. Among all the magnetic materials, magnetite (Fe_3O_4) is widely used because of its magnetic property, low toxicity, high biocompatibility and high Snoek's limit.³ In recent years, much work has been carried out on the EMI shielding performance of conductive polymer nanocomposites. For example, Wang *et al.* reported cobalt/PPy nanocomposites with tunable electromagnetic properties because of the coexistence of magnetic loss and dielectric loss of electromagnetic waves.³³ Sun *et al.* reported magnetic graphene with good EMI shielding performance.³ However, there is less work on the EMI shielding property of PPy with Fe_3O_4 nanocomposites. In our previous work, Fe_3O_4 nanoparticles coated with PPy have been successfully synthesized by the surface initiated polymerization (SIP) method.²⁶ The PPy functionalized Fe_3O_4 nanoparticles (PPy– Fe_3O_4) show enhanced dielectric, electrical and magnetic properties, indicating that these materials may have potential for EMI shielding application. In addition, it is well known that electromagnetic energy is transformed into joule thermal energy by EMI shielding materials. The generated joule thermal energy has the potential to ignite the materials. Thus, the flame retardant property is a vital parameter for EMI shielding materials in practical applications. Conductive polymers have shown great potential as flame retardant materials. For example, Zhang *et al.* reported PPy epoxy nanocomposites with reduced flammability.³⁴ Gu *et al.* reported the enhanced flame retardancy performance of epoxy nanocomposites with polyaniline stabilized silica nanoparticles.³⁵ Therefore, PPy could enhance the flame retardant property of the epoxy nanocomposites as well. However, as mentioned above, there is less work done on the epoxy nanocomposites with PPy– Fe_3O_4 nanoparticles.

Herein, epoxy nanocomposites with Fe_3O_4 –PPy nanoparticles have been reported with a higher electromagnetic wave absorption capacity and broader absorption bandwidth at high frequency compared to epoxy nanocomposites with PPy, Fe_3O_4 , and the two physically mixed fillers (PPy and Fe_3O_4). A scanning electron microscope was used to study the dispersion quality of the nanoparticles in the epoxy matrix. The electrical conductivity, magnetic property and electromagnetic wave absorption property were comparatively studied. In addition, the flame retardant property was evaluated by microscale combustion calorimetry to satisfy stringent industrial standards.

2. Experimental section

2.1 Materials

The bisphenol F epoxy (Epon 862) and a curing agent (EpiCure W) were provided by Miller-Stephenson Chemical Company, Inc. Pyrrole ($\text{C}_4\text{H}_5\text{N}$, $\geq 98\%$), ammonium persulfate (APS, $(\text{NH}_4)_2\text{S}_2\text{O}_8$, 98%) and *p*-toluene sulfonic acid (PTSA, $\text{C}_7\text{H}_8\text{O}_3\text{S}$, $\geq 98.5\%$) were purchased from Sigma-Aldrich. The Fe_3O_4 nanoparticles were obtained from Nanjing Emperor Nano Material Co., Ltd, China. All the chemicals were used as-received without any further treatment.

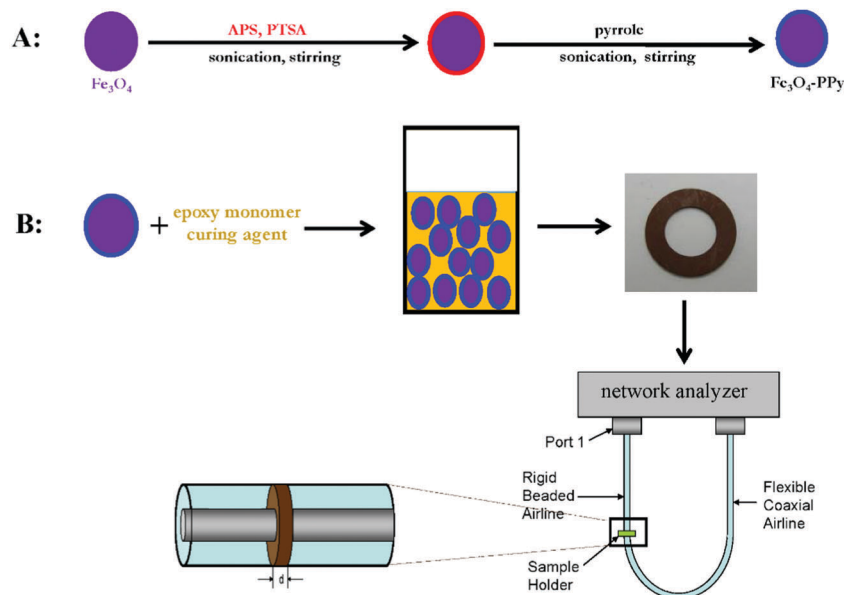
2.2 Synthesis of cured epoxy nanocomposites

The preparation of cured pure epoxy and epoxy nanocomposites with 5.0, 20.0, and 30.0 wt% Fe_3O_4 –PPy and 30.0 wt% as-received Fe_3O_4 nanoparticles was conducted. The SIP method for the surface functionalization of Fe_3O_4 nanoparticles by PPy was used,²⁶ as shown in Scheme 1(A). First, the Fe_3O_4 nanoparticles were dispersed in an aqueous solution containing PTSA (15 mmol) and APS (9 mmol) in 100 mL of deionized water by sonication for 1 hour and mechanical stirring in an ice-water bath. Second, the pyrrole solution (18 mmol, 25 mL deionized water) was mixed with the Fe_3O_4 nanoparticle suspension for polymerization under mechanical and ultrasonic stirring for an additional one and a half hours in an ice-water bath. The product was filtered and washed with deionized water several times. The epoxy nanocomposites with a physical mixture of 7.5 wt% PPy and 30.0 wt% as-received Fe_3O_4 nanoparticles, and epoxy nanocomposites with 7.5 wt% PPy were also prepared in this work.^{7,26} Here, the epoxy nanocomposites with PPy functionalized Fe_3O_4 are named as “epoxy/ Fe_3O_4 –PPy”. Epoxy nanocomposites with as-received Fe_3O_4 are named as “epoxy/ Fe_3O_4 ”. Epoxy nanocomposites with PPy are named as “epoxy/PPy” and the epoxy nanocomposites with a physical mixture of PPy and Fe_3O_4 are named as “epoxy/ Fe_3O_4 /PPy”. As shown in Scheme 1(B), the nanofillers were immersed in Epon 862 resin overnight to wet the nanoparticles. Then the suspension was mechanically stirred for 1 hour (600 rpm, Heidolph, RZR 2041). After that, the curing agent EpiCure W was added into the Epon resin nanosuspensions with a monomer/curing agent ratio of 100/26.5 for 1 hour mechanical stirring (200 rpm). Then the solution was mechanically stirred at 70 °C for 2 hours (200 rpm), which was essential to remove the bubbles and to prevent the sedimentation of the Fe_3O_4 nanoparticles during the curing process. Finally, the solutions were poured into silicone molds and cured at 120 °C for 5 hours.

2.3 Characterization

The morphology of the as-synthesized materials was examined using a FEI Helios NanoLab 600i scanning electron microscope (SEM, Hillsboro, OR). All the samples were sputter coated with a thin layer of carbon (about 3 nm) to ensure good imaging. The magnetic properties were investigated in a 9-Tesla Physical Property Measurement System (PPMS) by quantum design at room temperature.

The volume resistivity was measured by testing the DC resistance along the disc samples with a diameter of about



Scheme 1 Process for the fabrication of (A) PPy functionalized Fe_3O_4 nanoparticles, (B) epoxy Fe_3O_4 /PPy nanocomposites and the measurement of the electromagnetic wave absorption property.

60 mm using an Agilent 4339B high resistance meter. It allows us to measure the resistivity up to $10^{16} \Omega \text{ cm}$. A four-probe technique (C4S 4-Point Probe Head Cascade Microtech, the probe tips were made of tungsten carbide) was used for the measurement.

The tensile test was carried out following ASTM, D412-98a in a unidirectional tensile test machine (ZQ-20B-1 tensile strength testing system). The samples (dog bone shaped) were designed according to the ASTM standard requirement and prepared as described for the epoxy nanocomposites in the molds. A crosshead speed of 0.26 mm s^{-1} was used and the strain (mm mm^{-1}) was calculated by dividing the jogging displacement by the original gauge length.

The relative complex permeability ($\mu = \mu' + \mu''$) and permittivity ($\epsilon = \epsilon' + \epsilon''$) were measured using a network analyzer (Agilent Technologies model N5232A) based on the transmission line technique, as shown in Scheme 1(B). A donut shaped sample was cut from the as-prepared nanocomposites. The outer and inner diameters of the specimen were 7.00 and 3.04 mm, respectively. The specimen was then placed in a sample holder, which was located between the rigid beaded airline (APC-7) and the flexible coaxial airline (APC-7) that were connected to the network analyzer. The frequency of the electromagnetic waves tested was ranged from 100 MHz to 20 GHz. The permeability and permittivity were directly read using the software.

Microscale combustion calorimetry (MCC) was utilized to evaluate the fire hazards by measuring combustion behaviors of the milligram-sized samples using a Govmark Microscale Combustion Calorimeter (Model MCC-2) operated at a heating rate of $1 \text{ }^\circ\text{C s}^{-1}$ in the range from 90 to $650 \text{ }^\circ\text{C}$ in the pyrolysis zone. The samples were tested according to ASTM guidelines (ASTM D7309-07). Briefly, the combustion zone was set to $650 \text{ }^\circ\text{C}$. The oxygen and nitrogen flow rates were set to 20 and 80 mL min^{-1} , respectively. The heat release rate (HRR) in watts

per gram of the sample (W g^{-1}) was calculated from the oxygen depletion measurements. The heat release capacity (HRC) in J (g K)^{-1} was obtained by dividing the sum of the peak HRR by the heating rate in K s^{-1} . The total heat release (THR) in kJ g^{-1} was obtained by integrating the HRR curve. The char yield was obtained by weighing the sample before and after the test.

3. Results and discussion

3.1 SEM analysis

Fig. 1 shows the dispersion quality of the nanoparticles in the epoxy matrix. The surface with a “river-like pattern” is observed in the SEM microstructure of epoxy/(7.5 wt%)PPy, and the PPy nanoparticles are homogeneously distributed in the epoxy matrix, as shown in Fig. 1(a). For the epoxy/(30.0 wt%) Fe_3O_4 , the agglomeration of the Fe_3O_4 nanoparticles is obviously observed, which is marked by a red circle in Fig. 1(b). Compared with the epoxy/(7.5 wt%)PPy, the density of the “river-like” pattern appeared to be decreased in the SEM image of the epoxy/(30.0 wt%) Fe_3O_4 . It indicates that the Fe_3O_4 nanoparticles prevent the formation of a brittle fracture since the load is transferred from the weaker epoxy matrix to the stronger Fe_3O_4 nanoparticles. A similar phenomenon is also observed in the epoxy nanocomposites with silica nanoparticles.³⁵ For the epoxy nanocomposites with the physically mixed PPy and Fe_3O_4 nanoparticles, Fig. 1(c), the “river like” patterns totally disappeared. The dispersion quality of the Fe_3O_4 nanoparticles in the epoxy/(30.0 wt%) Fe_3O_4 /(7.5 wt%)PPy is much better than that of the epoxy/(30.0 wt%) Fe_3O_4 , indicating that the PPy nanoparticles enhanced the dispersion quality of the Fe_3O_4 nanoparticles in the epoxy matrix. The epoxy nanocomposites with PPy functionalized Fe_3O_4 , Fig. 1(d), show a relatively better dispersion quality

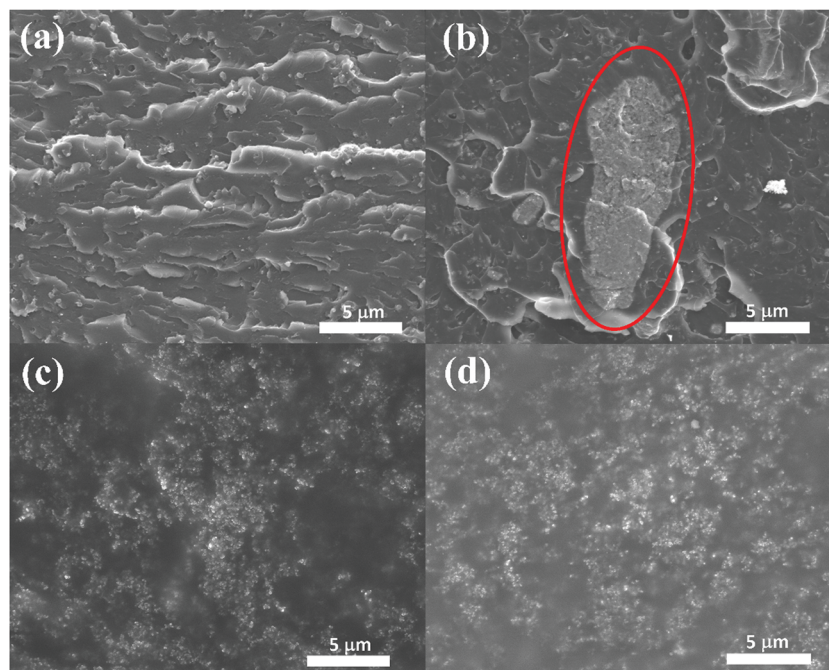


Fig. 1 SEM image of (a) epoxy/(7.5 wt%)PPy, (b) epoxy/(30.0 wt%)Fe₃O₄ (red cycle indicating the agglomeration of the Fe₃O₄), (c) epoxy/(30.0 wt%)Fe₃O₄/(7.5 wt%)PPy, and (d) epoxy/(30.0 wt%)Fe₃O₄-PPy.

than the epoxy/(30.0 wt%)Fe₃O₄/(7.5 wt%)PPy, due to the interaction between the PPy on the functionalized Fe₃O₄ nanoparticles and the epoxy matrix.⁷

3.2 Volume resistivity

Fig. 2 shows the volume resistivity of epoxy nanocomposites with different nanofillers at room temperature. The volume resistivity of the epoxy/(20.0 wt%)Fe₃O₄-PPy is about 1.2×10^{10} ohm cm, which is much higher than that of the epoxy/(7.5 wt%)PPy (about 9.9×10^4 ohm cm), epoxy/(30.0 wt%)Fe₃O₄/(7.5 wt%)PPy (about 2.9×10^4 ohm cm), and epoxy/(30.0 wt%)Fe₃O₄-PPy (about 9.3×10^5 ohm cm). Even though the volume resistivity of the epoxy/(30.0 wt%)Fe₃O₄-PPy is a little higher than that of the epoxy/(7.5 wt%)PPy and the epoxy/(30.0 wt%)Fe₃O₄/(7.5 wt%)PPy, the volume resistivity decreased by 5 orders of magnitude compared with that of the epoxy/(20.0 wt%)Fe₃O₄-PPy nanocomposites, indicating that the electrical conductivity is transferred from insulating materials to semiconductor materials.^{36–38}

3.3 Magnetic properties

Fig. 3 shows the magnetization curves of the epoxy/(30.0 wt%)-Fe₃O₄-PPy, epoxy/(30.0 wt%)Fe₃O₄, and epoxy/(30.0 wt%)Fe₃O₄/(7.5 wt%)PPy, respectively. For all the samples, no hysteresis loop, *i.e.*, zero coercivity (H_c), is observed (see the right inset picture in Fig. 3), indicating a superparamagnetic behavior of all the samples. The saturation magnetization (M_s) can be obtained by the extrapolated saturation magnetization from the intercept of $M-H^{-1}$ at high magnetic field.^{39–42} The obtained M_s values are 19.9, 15.9, and 16.0 emu g⁻¹ for epoxy/(30.0 wt%)Fe₃O₄-PPy, epoxy/(30.0 wt%)Fe₃O₄, and epoxy/(30.0 wt%)Fe₃O₄/(7.5 wt%)PPy, respectively. Based on the M_s value of 60.8 emu g⁻¹ for the Fe₃O₄

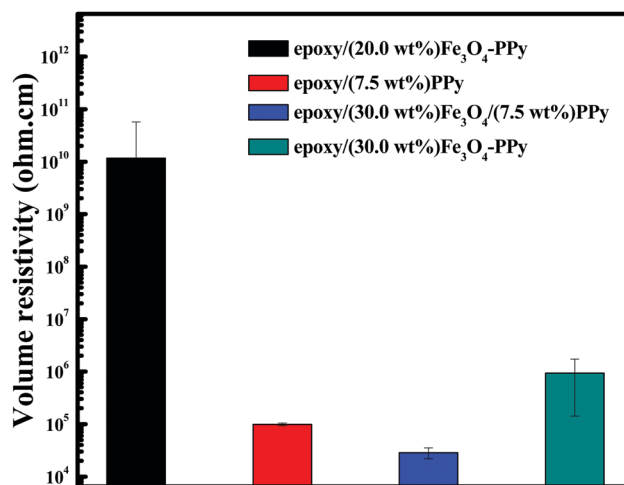


Fig. 2 Volume resistivity of epoxy/(20.0 wt%)Fe₃O₄-PPy; epoxy/(7.5 wt%)PPy; epoxy/(30.0 wt%)Fe₃O₄/(7.5 wt%)PPy; epoxy/(30.0 wt%)Fe₃O₄-PPy.

nanoparticles in our previous report,⁷ the particle loading values in the epoxy/(30.0 wt%)Fe₃O₄-PPy, epoxy/(30.0 wt%)Fe₃O₄, and epoxy/(30.0 wt%)Fe₃O₄/(7.5 wt%)PPy are 32.7, 26.2, and 26.3 wt%, respectively. They are consistent with our initial nanoparticle loading value of 30.0 wt%. The same phenomenon was observed in the SiC-Fe₃O₄ hybrid nanowires.⁴³ For a superparamagnetic system, the magnetic properties can be studied using the Langevin eqn (1):²⁶

$$\frac{M}{M_s} = \coth(aH) - \frac{1}{(aH)} \quad (1)$$

where M is the magnetization (emu g⁻¹) of the materials under magnetic field (H , Oe) and a (T⁻¹) is related to the electron spin

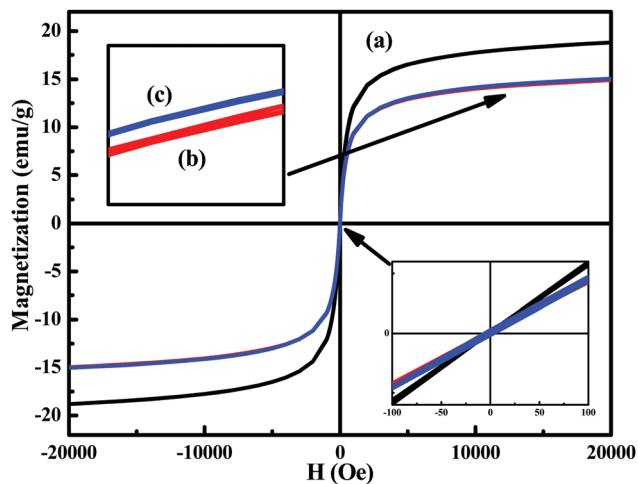


Fig. 3 Room temperature magnetization as a function of magnetic field for (a) epoxy/(30.0 wt%)Fe₃O₄-PPy, (b) epoxy/(30.0 wt%)Fe₃O₄, and (c) epoxy/(30.0 wt%)Fe₃O₄/(7.5 wt%)PPy, respectively.

magnetic moment m (μ_B) of the individual molecule as described in eqn (2):

$$a = \frac{m}{k_B T} \quad (2)$$

where k_B is the Boltzmann constant and T is the absolute temperature. The values of parameter a calculated using the polymath software for epoxy/(30.0 wt%)Fe₃O₄-PPy, epoxy/(30.0 wt%)Fe₃O₄, and epoxy/(30.0 wt%)Fe₃O₄/(7.5 wt%)PPy are 3.5, 3.3 and 3.3 T^{-1} , respectively. Based on eqn (2), the values of m for epoxy/(30.0 wt%)Fe₃O₄-PPy, epoxy/(30.0 wt%)Fe₃O₄, and epoxy/(30.0 wt%)Fe₃O₄/(7.5 wt%)PPy are 1.40, 1.32 and 1.32 μ_B , respectively. In our previous work, the m of the as-received Fe₃O₄ nanoparticles was found to be 1.19 μ_B .⁷ Therefore, the PPy and epoxy matrix have little effect on the magnetic moment of the Fe₃O₄ nanoparticles, no matter that the Fe₃O₄ nanoparticles are coated with PPy or physically mixed with PPy in the epoxy matrix.

3.4 Mechanical properties

Fig. 4 shows the tensile stress-strain curve of the cured epoxy nanocomposites. The tensile strength of epoxy/(7.5 wt%)PPy is 70.76 MPa, which is much higher than that of the other three magnetic epoxy nanocomposites in this work. The tensile strength of epoxy/(30.0 wt%)Fe₃O₄ is 31.45 MPa, which is the same as that of the epoxy nanocomposites with PPy functionalized Fe₃O₄ (The tensile strength is 30.65 MPa.). In the previous work, the conductive polymer could serve as a coupling agent between the epoxy matrix and nanoparticles which could enhance the mechanical property of the epoxy nanocomposites.^{7,44} However, due to the high loading of Fe₃O₄/PPy in the epoxy matrix, the epoxy/(30.0 wt%)Fe₃O₄-PPy did not show enhanced mechanical properties compared with epoxy/(30.0 wt%)Fe₃O₄.⁷ And the tensile strength of epoxy/(30.0 wt%)Fe₃O₄/(7.5 wt%)PPy is only 15.83 MPa, which is lower than that of epoxy/(30.0 wt%)Fe₃O₄, because except 30.0 wt% Fe₃O₄, 7.5 wt% PPy is also added into the epoxy. The Young's modulus is the slope of the stress-strain curve at the

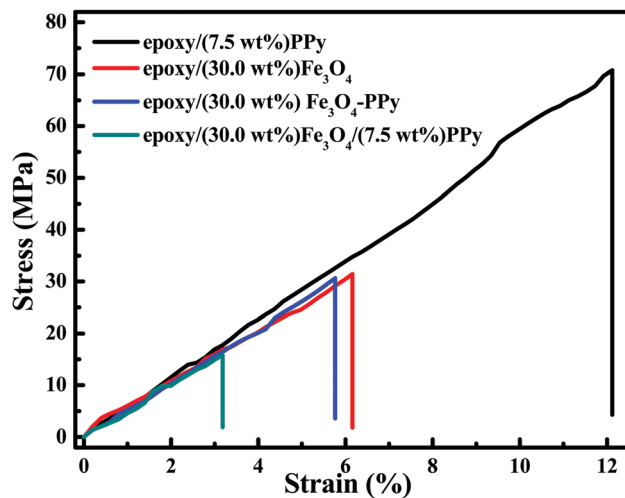


Fig. 4 Stress-strain curves of epoxy/(7.5 wt%)PPy, epoxy/(30.0 wt%)Fe₃O₄, epoxy/(30.0 wt%)Fe₃O₄-PPy and epoxy/(30.0 wt%)Fe₃O₄/(7.5 wt%)PPy, respectively.

elastic portion. The Young's modulus of epoxy/(30.0 wt%)Fe₃O₄ is larger than that of epoxy/(7.5 wt%)PPy, and epoxy/(30.0 wt%)Fe₃O₄/(7.5 wt%)PPy shows a larger Young's modulus than epoxy/(30.0 wt%)Fe₃O₄-PPy. The variation in elongation-to-break shows an opposite trend as compared to the change in Young's modulus.⁶ The toughness can be determined by integrating the stress-strain curve ($422.44 \text{ J m}^{-3} \times 10^4$ for epoxy/(7.5 wt%)PPy > $98.77 \text{ J m}^{-3} \times 10^4$ for epoxy/(30.0 wt%)Fe₃O₄ > $86.27 \text{ J m}^{-3} \times 10^4$ for epoxy/(30.0 wt%)Fe₃O₄-PPy > and $25.24 \text{ J m}^{-3} \times 10^4$ for epoxy/(30.0 wt%)Fe₃O₄/(7.5 wt%)PPy). The toughness shows the same trend as the elongation-to-break.

3.5 Microwave absorption performance

Fig. 5 shows the frequency dependent real part (ϵ') and imaginary part (ϵ'') of the relative complex permittivity ($\epsilon_r = \epsilon' + i\epsilon''$); ϵ' and ϵ'' stand for storage and loss capability of electrical energy. And the frequency dependent real part (μ') and imaginary part (μ'') of the relative complex permeability ($\mu_r = \mu' + i\mu''$), the μ' and μ'' stand for the storage and loss capability of magnetic energy. The ϵ' for all the samples decreases with increasing the frequency. The ϵ' value decreases from 11 to 4 for epoxy/(20.0 wt%)Fe₃O₄-PPy as shown in Fig. 5(a). The ϵ' value of epoxy/(30.0 wt%)Fe₃O₄ is almost constant in the measured frequency, Fig. 5(b). For epoxy/(7.5 wt%)PPy and epoxy/(30.0 wt%)Fe₃O₄-PPy, the ϵ' value decreases from 40 to 8 and from 22 to 9 as shown in Fig. 5(c and d), respectively. An obvious peak at around 13 GHz is observed for the ϵ'' value in the epoxy/(20.0 wt%)Fe₃O₄-PPy, Fig. 5(a), which is due to the resonance behavior of Fe₃O₄ in the epoxy/(20.0 wt%)Fe₃O₄-PPy nanocomposites.⁴⁵ A similar phenomenon is also observed in the Co/C nanoparticles.⁴⁶ The ϵ'' value of the other three samples is almost constant within the measured frequency. And the ϵ'' value of epoxy/(7.5 wt%)PPy is larger than that of the other three samples. According to the free electron theory, the σ (electrical conductivity) is related to ϵ'' and is expressed using eqn (3):^{46,47}

$$\sigma = 2\pi\epsilon_0\epsilon''f \quad (3)$$

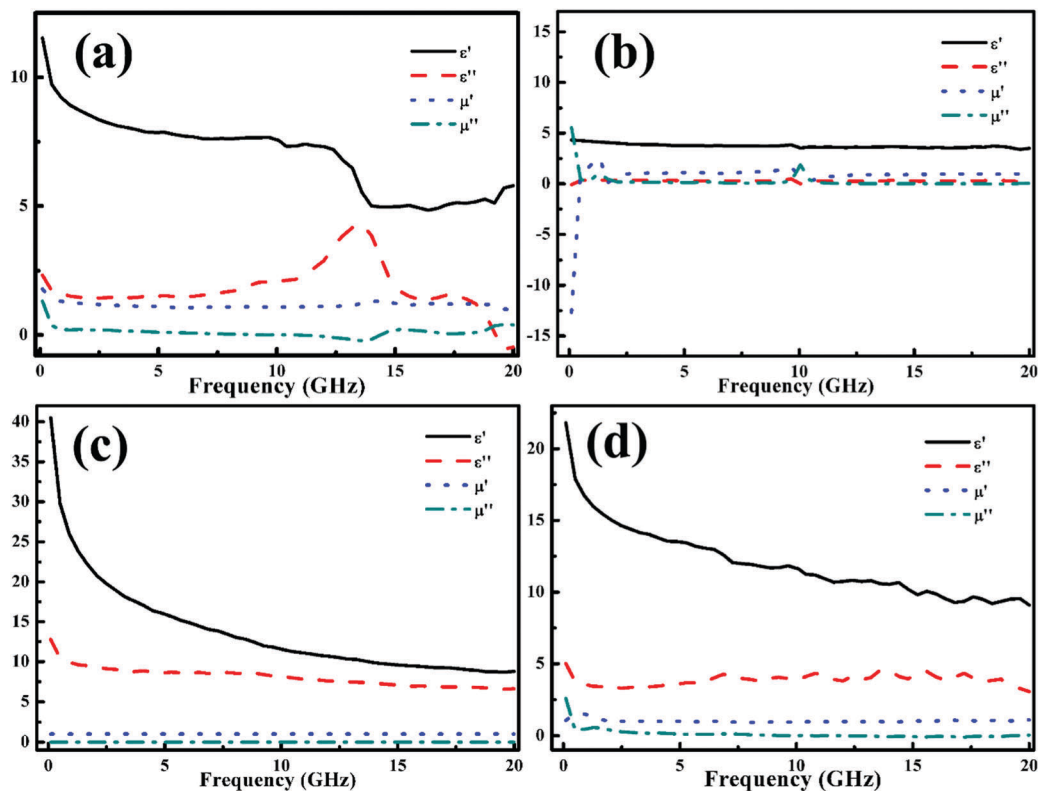


Fig. 5 Permittivity and permeability vs. frequency of (a) epoxy/(20.0 wt%)Fe₃O₄-PPy, (b) epoxy/(30.0 wt%)Fe₃O₄, (c) epoxy/(7.5 wt%)PPy, and (d) epoxy/(30.0 wt%)Fe₃O₄-PPy.

where ϵ_0 is the free space permittivity and f is the frequency. The ϵ'' of epoxy/(7.5 wt% PPy) is larger than those of the epoxy nanocomposites with as-received Fe₃O₄ and Fe₃O₄-PPy nanoparticles; therefore the epoxy/(7.5 wt% PPy) also shows a higher electrical conductivity, which is consistent with the result in the volume resistivity section. It can be seen in Fig. 5(a) that the μ' and μ'' values of epoxy/(20.0 wt%)Fe₃O₄-PPy are slightly changed within the measured frequency (μ' about 1–1.7 and μ'' about 0–1.3). For epoxy/(30.0 wt%)Fe₃O₄, the μ' and μ'' values are almost constant; however, the peaks are observed at around 10 GHz as shown in Fig. 5(b). The μ' value is 1 and the μ'' value is 0 as shown in Fig. 5(c) since there is no magnetic component in the epoxy/(7.5 wt%)PPy. As can be seen in Fig. 5(d), the μ' value is almost constant at 1 and the μ'' value slightly decreases from 0.6 to 0.

The reflection loss (RL) is calculated based on the transmission line theory to study the microwave absorption properties.^{3a} The RL of the electromagnetic radiation under normal wave incidence on a single layer material surface backed by a perfect conductor can be defined using eqn (4):^{5,48}

$$RL = -20 \log_{10} \left| \frac{Z - 1}{Z + 1} \right| \quad (4)$$

where Z represents the input impedance at the interface of free space and tested materials. The Z can be expressed as eqn (5):⁵

$$Z = \sqrt{\frac{\mu_r}{\epsilon_r}} \tanh \left(-i \frac{2\pi f d}{c} \sqrt{\mu_r \epsilon_r} \right) \quad (5)$$

f is the frequency of the electromagnetic wave, d is the thickness of the tested material, and c is the velocity of electromagnetic waves in free space.⁴⁹ The RL of these epoxy samples with a thickness varying from 1.2 to 3.0 mm is calculated and displayed in Fig. 6. Generally, the RL below -10 , -20 and -30 dB is 90.0, 99.0 and 99.9% attenuation of the incident electromagnetic wave, respectively. The electromagnetic wave absorption properties of these epoxy samples are summarized in Table 1. As can be seen in Fig. 6(a), the minimum RL of epoxy/(20.0 wt%)Fe₃O₄-PPy is -16.4 dB when the thickness is 2.4 mm, and the absorption bandwidth below -10 dB is 5.9 GHz. However, the bandwidth below -20 dB is 0 GHz. For epoxy/(30.0 wt%)Fe₃O₄, Fig. 6(b), although the minimum RL value is -17.8 dB, the absorption bandwidth below -10 dB is 0 GHz. For epoxy/(7.5 wt%)PPy, Fig. 6(c), the absorption bandwidth below -10 dB is only 1.2 GHz, and below -20 dB is 0 GHz. Even though the above three samples show electromagnetic wave absorption, the absorption bandwidth below -10 and -20 dB is not good enough for real EMI shielding application. Compared with the above three samples, the epoxy/(30.0 wt%)Fe₃O₄-PPy as shown in Fig. 6(d), shows a much enhanced electromagnetic wave absorption property. The minimum RL value even reaches -35.7 dB, whereas the RL below -10 dB is 4 GHz and the RL below -20 dB is 0.8 GHz. The RL of the epoxy/(30.0 wt%)Fe₃O₄/(7.5 wt%)PPy is shown in Fig. S1 (ESI[†]), and the absorption bandwidth below -10 and -20 dB is almost 0 GHz. With the same loading of Fe₃O₄ nanoparticles and PPy, the electromagnetic wave

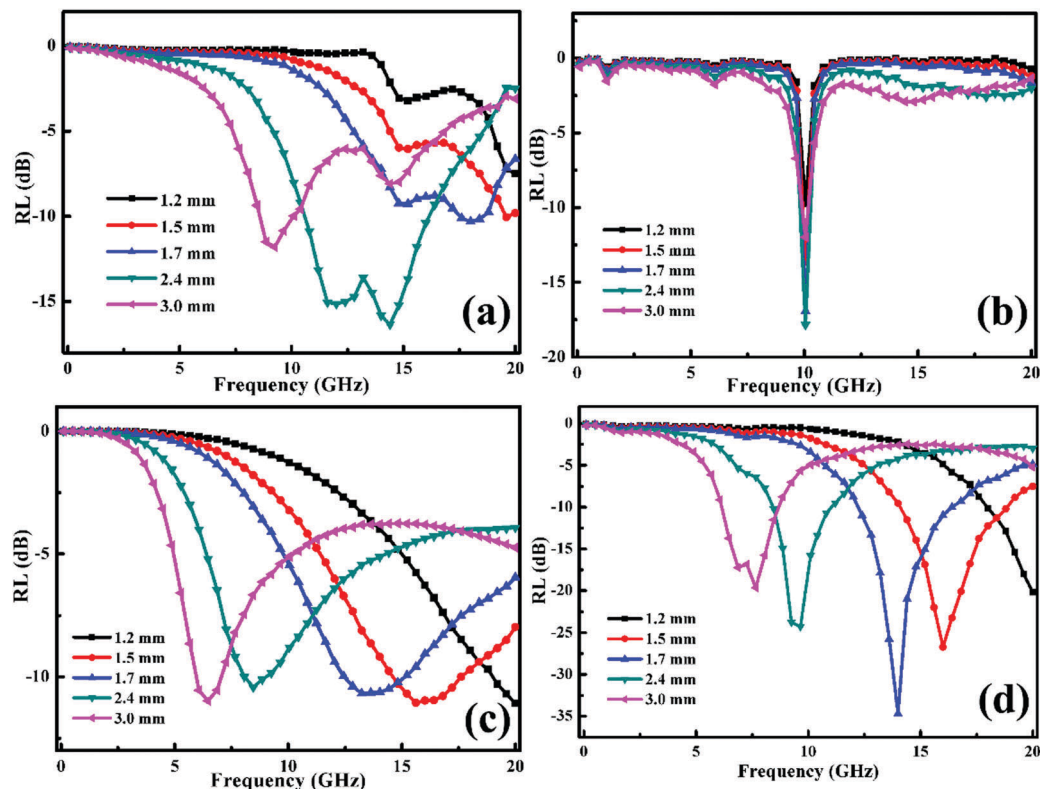


Fig. 6 Dependence of RL on the thickness of the absorption layer within the frequency range of 0.1–20.0 GHz: (a) epoxy/(20.0 wt%)Fe₃O₄-PPy, (b) epoxy/(30.0 wt%)Fe₃O₄, (c) epoxy/(7.5 wt%)PPy and (d) epoxy/(30.0 wt%)Fe₃O₄-PPy.

absorption performance of epoxy with a physical mixture of Fe₃O₄ and PPy is very poor; however, the epoxy with PPy coated Fe₃O₄ nanoparticles shows a much enhanced electromagnetic wave absorption performance mainly because the PPy coated Fe₃O₄ nanoparticles make a better electromagnetic matching.⁵⁰

There are many factors that influence the electromagnetic absorption properties, such as dielectric loss, magnetic loss and characteristic impedance.^{51–54} Based on eqn (5), at the same thickness, if the dielectric loss contribution and magnetic loss contribution were well matched, the material would show an enhanced electromagnetic wave absorption property. The electromagnetic energy is transformed into joule thermal energy during the polarization process for the dielectric material, which results in the microwave attenuation. This could be described by the Debye relaxation using eqn (6):⁴⁵

$$(\epsilon' - \epsilon_\infty)^2 + (\epsilon'')^2 = (\epsilon_s - \epsilon_\infty)^2 \quad (6)$$

where ϵ_s is the static permittivity and ϵ_∞ is the relative dielectric permittivity at the high-frequency limit. The plot of ϵ'' vs. ϵ' would be semicircle, denoted as the Debye semicircle. Each semicircle corresponds to a Debye dipolar relaxation. Fig. 7 shows the $\epsilon' - \epsilon''$ curves of the epoxy samples. It is obvious that the epoxy/(30.0 wt%)Fe₃O₄ nanocomposites present a totally disordered curve with no semicircle and dielectric relaxation.⁴⁵ For epoxy/(20.0 wt%)Fe₃O₄-PPy and epoxy/(30.0 wt%)Fe₃O₄-PPy, there are two semicircles observed, which correspond to two dielectric relaxation processes. However, there is one semicircle observed in the epoxy/(7.5 wt%)PPy nanocomposites. From the above results, it is observed that the PPy functionalized Fe₃O₄ epoxy nanocomposites enhanced the EMI shielding performance, because of the interface polarizations between Fe₃O₄ and PPy, and between PPy and the epoxy matrix.⁷ However, there is only one interface polarization between PPy and epoxy, and there is no magnetic loss in the epoxy/(7.5 wt%)PPy nanocomposites. Therefore, the epoxy/(7.5 wt%)PPy nanocomposites show a poor electromagnetic absorption property.

It is well known that the magnetic loss is mainly induced by the natural resonance, exchange resonance and eddy current loss.^{46,54,55} The magnetic loss is usually induced by the eddy current loss in a high frequency region, which can be evaluated using eqn (7):⁵

$$\mu'' = 2\pi\mu_0(\mu')^2\sigma d^2 f/3 \quad (7)$$

Table 1 Microwave absorption properties of HRR as a function of temperature for epoxy/(20.0 wt%)Fe₃O₄-PPy, epoxy/(30.0 wt%)Fe₃O₄, epoxy/(7.5 wt%)PPy and epoxy/(30.0 wt%)Fe₃O₄-PPy

Sample	Minimum RL value (dB)	Thickness (mm)	Absorption bandwidth (≤ 10 dB)	Absorption bandwidth (≤ 20 dB)
20.0 wt% of Fe ₃ O ₄ -PPy	-16.4	2.4	5.9	0
30.0 wt% of Fe ₃ O ₄	-17.8	2.4	0	0
7.5 wt% PPy	-11.0	1.5	1.2	0
30.0 wt% Fe ₃ O ₄ -PPy	-35.7	1.7	4	0.8

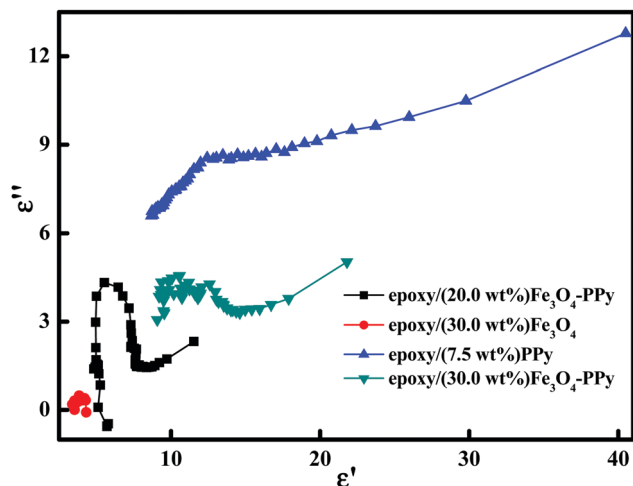


Fig. 7 Frequency dependence of the Cole-Cole semicircles for the epoxy/(20.0 wt%)Fe₃O₄-PPy, epoxy/(30.0 wt%)Fe₃O₄, epoxy/(7.5 wt%)PPy and epoxy/(30.0 wt%)Fe₃O₄-PPy.

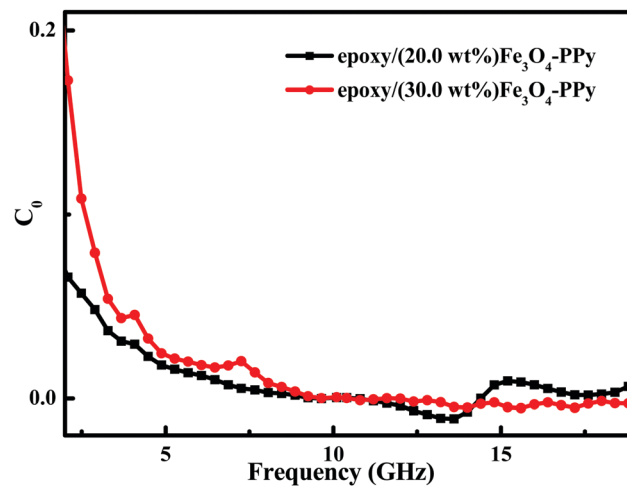


Fig. 8 C_0 - f curves of epoxy/(20.0 wt%)Fe₃O₄-PPy and epoxy/(30.0 wt%)Fe₃O₄-PPy.

where σ (S m⁻¹) is the electrical conductivity and μ_0 (H m⁻¹) is the permeability in vacuum. In general, if the reflection loss is induced by the eddy current, the values of C_0 ($C_0 = \mu''(\mu')^{-2}f^{-1}$) are constant when the frequency is changing. It is obvious that C_0 of the epoxy with PPy functionalized Fe₃O₄ nanoparticles is constant at high frequency, Fig. 8. Due to the higher loading of Fe₃O₄-PPy nanoparticles in epoxy/(30.0 wt%)Fe₃O₄-PPy, the C_0 of epoxy/(30.0 wt%)Fe₃O₄-PPy nanocomposites is relatively more constant than that of epoxy/(20.0 wt%)Fe₃O₄-PPy nanocomposites. For epoxy/(30.0 wt%)Fe₃O₄ in Fig. S2 (ESI[†]), the C_0 is constant; however, the electromagnetic absorption ability is very poor. It indicates that the magnetic loss did not match well with the dielectric loss and limited the electromagnetic absorption.⁴⁵

On the other hand, better magnetic absorption property is due to the enhanced anisotropic energy (H_a) that can be presented as eqn (8):⁸

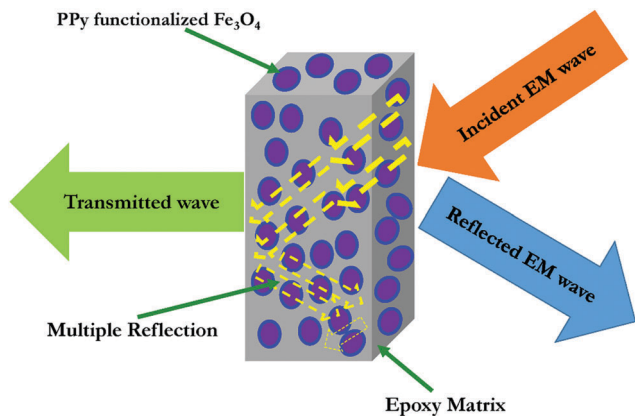
$$H_a = 4|K_1|/3\mu_0M_s \quad (8)$$

where $|K_1|$ is the anisotropic coefficient. A higher anisotropic energy, a better electromagnetic absorption. The calculated M_s values for epoxy/(20.0 wt%)Fe₃O₄-PPy, epoxy/(30.0 wt%)Fe₃O₄, epoxy/(30.0 wt%)Fe₃O₄/(7.5 wt%)PPy, and epoxy/(30.0 wt%)Fe₃O₄-PPy are 13.1, 15.9, 16.0 and 19.9 emu g⁻¹, respectively.⁷ The H_a of epoxy/(20.0 wt%)Fe₃O₄-PPy is higher than the H_a of the other three samples. The higher H_a is helpful to improve the electromagnetic wave absorption property.⁸ Therefore, epoxy/(20.0 wt%)Fe₃O₄-PPy shows better electromagnetic absorption properties than epoxy/(30.0 wt%)Fe₃O₄, and epoxy/(30.0 wt%)Fe₃O₄/(7.5 wt%)PPy nanocomposites. However, even the H_a of epoxy/(20.0 wt%)Fe₃O₄-PPy is higher than that of epoxy/(30.0 wt%)Fe₃O₄-PPy, and the electromagnetic wave absorption property of epoxy/(30.0 wt%)Fe₃O₄-PPy is much better, indicating that there are other effects (such as dielectric loss and magnetic loss) on the electromagnetic absorption property. In other words, the epoxy nanocomposites with PPy functionalized Fe₃O₄ show enhanced electromagnetic absorption

properties due to the increased interface area formed between PPy and Fe₃O₄ and the fact that the magnetic loss well matches the dielectric loss. The eddy current loss, enhanced anisotropic energy and interface polarization have all contributed to the enhanced electromagnetic wave absorption of epoxy/Fe₃O₄-PPy nanocomposites. The proposed EMI shielding mechanism is shown in Scheme 2. The EM wave is attenuated by the nanocomposites, and the attenuation of an EM wave includes absorption, reflection, and multiple reflections.^{56,57} When a higher amount of Fe₃O₄-PPy nanoparticles is loaded, a better electromagnetic absorption is achieved.

3.6 Combustion behavior and fire hazard

Fig. 9 shows the HRR as a function of temperature for pure epoxy and epoxy/(30.0 wt%)Fe₃O₄-PPy nanocomposites. Table 2 shows the related heat release parameters. The HRR is one single important parameter to estimate the fire hazard of the flammable materials.⁵⁸ During fires, the materials with a higher HRR would generate a heat flux, which is very dangerous. Therefore, it is important to decrease the HRR. For pure epoxy, the peak HRR is 470.3 W g⁻¹ at 397.4 °C, the HR capacity and total HR are 453.0 J g⁻¹ K⁻¹ and 25.5 kJ g⁻¹. The HRR of pure epoxy is much lower than that of the thermoplastic material polypropylene with a HRR of 1513.0 W g⁻¹.⁵ The initial thermal decomposition temperature of epoxy/(30.0 wt%)Fe₃O₄-PPy nanocomposites is lower than that of pure epoxy, which is consistent with the thermal stability property.⁷ Compared with pure epoxy, the peak HRR at 386.5 °C of epoxy/(30.0 wt%)Fe₃O₄-PPy nanocomposites decreased to 292 W g⁻¹. And the HRR reduction is 36.4%. Apparently, the reduced peak HRR is due to the dilution of pure epoxy after adding the nanoparticles. In our previous work, there is covalent bonding formed between PPy on the surface of Fe₃O₄ and the epoxy matrix.⁷ The formed covalent bonding can postpone the degradation of the materials. A similar phenomenon was also observed in the polyaniline epoxy nanocomposites and in other polymers.⁵⁹⁻⁶² The char residue of epoxy/(30.0 wt%)Fe₃O₄-PPy nanocomposites (49.2%) is much



Scheme 2 Schematic illustrations of the EMI shielding performance of epoxy/ Fe_3O_4 -PPy nanocomposites.

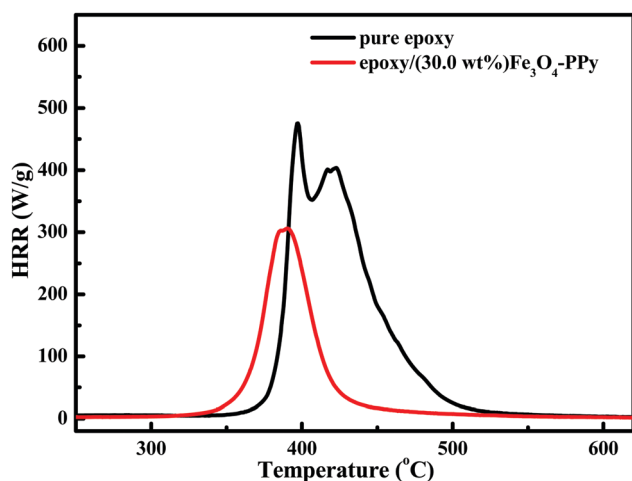


Fig. 9 HRR as a function of temperature for pure epoxy and epoxy/(30.0 wt%) Fe_3O_4 -PPy.

higher than that of pure epoxy (6.2%). The char yield is considered a characteristic of flame retardancy.^{34,63} The formed char layer on the surface of the materials would keep the heat transferred from the heat source to the inner material and obstruct the distribution of combustible gases produced from the materials during the test as well.^{60,64,65} On the other hand, the epoxy/(30.0 wt%) Fe_3O_4 -PPy nanocomposites contain PPy as well as the nitrogen element. Normally, the nitrogen-containing compounds are gas sources; this kind of material can produce incombustible gases without toxic smoke during their degradation at high temperature.^{35,60} The produced gas can dilute the concentration of oxygen near the flame.⁶⁶ Therefore, the epoxy/(30.0 wt%) Fe_3O_4 -PPy nanocomposites show a decreased HRR and enhanced flame retardancy.

Table 2 Heat release parameters of pure epoxy and epoxy/(30.0 wt%) Fe_3O_4 -PPy

Sample	PHRR (W g^{-1})	PHRR reduction (%)	THR (kJ g^{-1})	HR capacity ($\text{J g}^{-1} \text{K}^{-1}$)	Char (%)
Pure epoxy	470.3	—	25.5	453.0	6.2
Epoxy/(30.0 wt%) Fe_3O_4 -PPy	299.2	36.4	12.3	292.0	49.2

4. Conclusion

The epoxy nanocomposites reinforced with PPy functionalized Fe_3O_4 nanoparticles prepared by the SIP method show enhanced electromagnetic wave absorption performance. The magneto-resistance behavior was observed in the PPy coated magnetic nanoparticles; thus, these magnetic epoxy nanocomposites have the potential for other applications such as magnetic sensors and information storage.^{26,67} The epoxy/(30.0 wt%) Fe_3O_4 -PPy nanocomposites with a thickness of 1.7 mm show good electromagnetic wave absorption performance (the absorption bandwidth of $\text{RL} < -10$ dB is 4.0 GHz and the absorption bandwidth of $\text{RL} < -20$ dB is 0.8 GHz) with a minimum RL value of -35.7 dB. The enhanced electromagnetic wave absorption performance indicates that the dielectric loss better matches with magnetic loss, compared with epoxy with pure PPy or the as-received Fe_3O_4 nanoparticles. The increased interface area, eddy current loss and increased H_a contribute to the improved electromagnetic wave absorption performance. According to the requirements of the Federal Communications Commission, our materials failed to meet the requirement of the common housing electronic equipment ($\text{RL} < -40$ dB),^{68,69} however, if the particle loading is further increased, we believe that our epoxy nanocomposites have the potential to reach that requirement. Meanwhile, the combusted amount of the epoxy nanocomposites is almost half of the combusted amount of pure epoxy, which meets the requirement of the National Institute of Standards and Technology.⁷⁰ Therefore, the significantly reduced flammability makes these nanocomposites suitable for safer electromagnetic wave absorbers to satisfy stringent industrial standards. In other words, upon addition of the nanoparticles, the epoxy nanocomposites will have broader applications such as in aeronautics and aerospace industry, automobile industry, as anti-corrosion coatings, and high voltage applications.²¹

Acknowledgements

This project was financially supported by the start-up funds of the University of Tennessee, Knoxville and the American Chemical Society Petroleum Research Fund (ACS PRF# 53930-ND6). D. P. Young acknowledges the support from the NSF under Grant No. DMR 13-06392. H. Song acknowledges the support from the China Scholarship Council (CSC) program. T. Ding acknowledges the support from the Science and Technology Development Program of Henan Province (152102210052).

References

- J. Liang, Y. Wang, Y. Huang, Y. Ma, Z. Liu, J. Cai, C. Zhang, H. Gao and Y. Chen, *Carbon*, 2009, **47**, 922–925.
- (a) C. Alippi, *CAAI Trans. Intelligence Technology*, 2016, **1**, 1–3; (b) Z. Sun, L. Zhang, F. Dang, Y. Liu, Z. Fei, Q. Shao, H. Lin, J. Guo, L. Xiang, N. Yerra and Z. Guo, *CrystEngComm*, 2017, DOI: 10.1039/C7CE00279C.
- X. Sun, J. He, G. Li, J. Tang, T. Wang, Y. Guo and H. Xue, *J. Mater. Chem. C*, 2013, **1**, 765–777.

- 4 H.-M. Xiao and S.-Y. Fu, *CrystEngComm*, 2014, **16**, 2097–2112.
- 5 Q. He, T. Yuan, X. Zhang, X. Yan, J. Guo, D. Ding, M. A. Khan, D. P. Young, A. Khasanov, Z. Luo, J. Liu, T. D. Shen, X. Liu, S. Wei and Z. Guo, *J. Phys. Chem. C*, 2014, **118**, 24784–24796.
- 6 H. Gu, J. Guo, H. Wei, X. Yan, D. Ding, X. Zhang, Q. He, S. Tadakamalla, X. Wang, T. C. Ho, S. Wei and Z. Guo, *J. Mater. Chem. C*, 2015, **3**, 8152–8165.
- 7 J. Guo, X. Zhang, H. Gu, Y. Wang, X. Yan, D. Ding, J. Long, S. Tadakamalla, Q. Wang, M. A. Khan, J. Liu, X. Zhang, B. L. Weeks, L. Sun, D. P. Young, S. Wei and Z. Guo, *RSC Adv.*, 2014, **4**, 36560–36572.
- 8 (a) J. Zhu, S. Wei, N. Haldolaarachchige, D. P. Young and Z. Guo, *J. Phys. Chem. C*, 2011, **115**, 15304–15310; (b) Y. Ma, J. Dai, L. Wu, G. Fang and Z. Guo, *Polymer*, 2017, **114**, 113–121.
- 9 J. Guo, J. Long, D. Ding, Q. Wang, Y. Shan, A. Umar, X. Zhang, B. L. Weeks, S. Wei and Z. Guo, *RSC Adv.*, 2016, **6**, 21187–21192.
- 10 H. Jin, Q. Chen, Z. Chen, Y. Hu and J. Zhang, *CAAI Trans. Intelligence Technology*, 2016, **1**, 104–113.
- 11 H. Liu, M. Dong, W. Huang, J. Gao, K. Dai, J. Guo, G. Zheng, C. Liu, C. Shen and Z. Guo, *J. Mater. Chem. C*, 2017, **5**, 73–83.
- 12 H. Liu, J. Gao, W. Huang, K. Dai, G. Zheng, C. Liu, C. Shen, X. Yan, J. Guo and Z. Guo, *Nanoscale*, 2016, **8**, 12977–12989.
- 13 X. Zhang, H. Gao, M. Guo, G. Li, Y. Liu and D. Li, *CAAI Trans. Intelligence Technology*, 2016, **1**, 4–13.
- 14 J. Gu, Y. Guo, X. Yang, C. Liang, W. Geng, L. Tang, N. Li and Q. Zhang, *Composites, Part A*, 2017, **95**, 267–273.
- 15 J. Gu, Q. Zhang, Y. Tang, J. Zhang, J. Kong, J. Dang, H. Zhang and X. Wang, *Surf. Coat. Technol.*, 2008, **202**, 2891–2896.
- 16 L.-C. Jia, D.-X. Yan, C.-H. Cui, X. Jiang, X. Ji and Z.-M. Li, *J. Mater. Chem. C*, 2015, **3**, 9369–9378.
- 17 D.-X. Yan, H. Pang, B. Li, R. Vajtai, L. Xu, P.-G. Ren, J.-H. Wang and Z.-M. Li, *Adv. Funct. Mater.*, 2015, **25**, 559–566.
- 18 C.-H. Cui, D.-X. Yan, H. Pang, X. Xu, L.-C. Jia and Z.-M. Li, *ACS Sustainable Chem. Eng.*, 2016, **4**, 4137–4145.
- 19 J. Kong, Y. Tang, X. Zhang and J. Gu, *Polym. Bull.*, 2008, **60**, 229–236.
- 20 N. Tian, R. Ning and J. Kong, *Polymer*, 2016, **99**, 376–385.
- 21 H. Gu, C. Ma, J. Gu, J. Guo, X. Yan, J. Huang, Q. Zhang and Z. Guo, *J. Mater. Chem. C*, 2016, **4**, 5890–5906.
- 22 J. Gu, X. Yang, Z. Lv, N. Li, C. Liang and Q. Zhang, *Int. J. Heat Mass Transfer*, 2016, **92**, 15–22.
- 23 H. Gu, C. Ma, C. Liang, X. Meng, J. Gu and Z. Guo, *J. Mater. Chem. C*, 2017, **5**, 4275–4285.
- 24 J. Gu, C. Liang, X. Zhao, B. Gan, H. Qiu, Y. Guo, X. Yang, Q. Zhang and D.-Y. Wang, *Compos. Sci. Technol.*, 2017, **139**, 83–89.
- 25 B.-J. Kim, K.-M. Bae, Y. S. Lee, K.-H. An and S.-J. Park, *Surf. Coat. Technol.*, 2014, **242**, 125–131.
- 26 J. Guo, H. Gu, H. Wei, Q. Zhang, N. Haldolaarachchige, Y. Li, D. P. Young, S. Wei and Z. Guo, *J. Phys. Chem. C*, 2013, **117**, 10191–10202.
- 27 (a) L. Shao, X. Cheng, Z. Wang, J. Ma and Z. Guo, *J. Membr. Sci.*, 2014, **452**, 82–89; (b) X. Cheng, S. Ding, J. Guo, C. Zhang, Z. Guo and L. Shao, *J. Membr. Sci.*, 2017, **536**, 19–27.
- 28 H. Wei, C. He, J. Liu, H. Gu, Y. Wang, X. Yan, J. Guo, D. Ding, N. Z. Shen, X. Wang, S. Wei and Z. Guo, *Polymer*, 2015, **67**, 192–199.
- 29 (a) H. Wei, Y. Wang, J. Guo, X. Yan, R. O'Connor, X. Zhang, N. Z. Shen, B. L. Weeks, X. Huang, S. Wei and Z. Guo, *ChemElectroChem*, 2015, **2**, 119–126; (b) H. Wei, H. Gu, J. Guo, X. Yan, J. Liu, D. Cao, X. Wang, S. Wei and Z. Guo, Significantly Enhanced Energy Density of Magnetite/Polypyrrole Nanocomposite Capacitors at High Rates by Low Magnetic Fields, *Adv. Compos. Sci.*, 2017, in press.
- 30 X. Zhang, J. Zhu, N. Haldolaarachchige, J. Ryu, D. P. Young, S. Wei and Z. Guo, *Polymer*, 2012, **53**, 2109–2120.
- 31 S. H. Kim, S. H. Jang, S. W. Byun, J. Y. Lee, J. S. Joo, S. H. Jeong and M.-J. Park, *J. Appl. Polym. Sci.*, 2003, **87**, 1969–1974.
- 32 J. Avloni, R. Lau, M. Ouyang, L. Florio, A. R. Henn and A. Sparavigna, *J. Ind. Text.*, 2008, **38**, 55–68.
- 33 H. Wang, N. Ma, Z. Yan, L. Deng, J. He, Y. Hou, Y. Jiang and G. Yu, *Nanoscale*, 2015, **7**, 7189–7196.
- 34 X. Zhang, X. Yan, J. Guo, Z. Liu, D. Jiang, Q. He, H. Wei, H. Gu, H. A. Colorado, X. Zhang, S. Wei and Z. Guo, *J. Mater. Chem. C*, 2015, **3**, 162–176.
- 35 H. Gu, J. Guo, Q. He, S. Tadakamalla, X. Zhang, X. Yan, Y. Huang, H. A. Colorado, S. Wei and Z. Guo, *Ind. Eng. Chem. Res.*, 2013, **52**, 7718–7728.
- 36 A. Elschner, S. Kirchmeyer, W. Lövenich, U. Merker and K. Reuter, *PEDOT: principles and applications of an intrinsically conductive polymer*, CRC Press, 2011.
- 37 X. Guan, G. Zheng, K. Dai, C. Liu, X. Yan, C. Shen and Z. Guo, *ACS Appl. Mater. Interfaces*, 2016, **8**, 14150–14159.
- 38 Y.-S. Tang, J. Kong, J.-W. Gu and G.-Z. Liang, *Polym.-Plast. Technol. Eng.*, 2009, **48**, 359–366.
- 39 Z. Guo, L. L. Henry, V. Palshin and E. J. Podlaha, *J. Mater. Chem.*, 2006, **16**, 1772–1777.
- 40 J. Kong, M. Kong, X. Zhang, L. Chen and L. An, *ACS Appl. Mater. Interfaces*, 2013, **5**, 10367–10375.
- 41 J. Kong, T. Schmalz, G. Motz and A. H. E. Muller, *J. Mater. Chem. C*, 2013, **1**, 1507–1514.
- 42 W. Zhao, Y. Tang, J. Xi and J. Kong, *Appl. Surf. Sci.*, 2015, **326**, 276–284.
- 43 C. Liang, C. Liu, H. Wang, L. Wu, Z. Jiang, Y. Xu, B. Shen and Z. Wang, *J. Mater. Chem. A*, 2014, **2**, 16397–16402.
- 44 H. Gu, S. Tadakamalla, Y. Huang, H. A. Colorado, Z. Luo, N. Haldolaarachchige, D. P. Young, S. Wei and Z. Guo, *ACS Appl. Mater. Interfaces*, 2012, **4**, 5613–5624.
- 45 Y. Du, W. Liu, R. Qiang, Y. Wang, X. Han, J. Ma and P. Xu, *ACS Appl. Mater. Interfaces*, 2014, **6**, 12997–13006.
- 46 T. Liu, X. Xie, Y. Pang and S. Kobayashi, *J. Mater. Chem. C*, 2016, **4**, 1727–1735.
- 47 J. Gu, Z. Lv, Y. Wu, Y. Guo, L. Tian, H. Qiu, W. Li and Q. Zhang, *Composites, Part A*, 2017, **94**, 209–216.
- 48 J. Gu, W. Dong, S. Xu, Y. Tang, L. Ye and J. Kong, *Compos. Sci. Technol.*, 2017, **144**, 185–192.

- 49 W. Xie, X. Zhu, S. Yi, J. Kuang, H. Cheng, W. Tang and Y. Deng, *Mater. Des.*, 2016, **90**, 38–46.
- 50 Y. Li, G. Chen, Q. Li, G. Qiu and X. Liu, *J. Alloys Compd.*, 2011, **509**, 4104–4107.
- 51 B. Lu, X. L. Dong, H. Huang, X. F. Zhang, X. G. Zhu, J. P. Lei and J. P. Sun, *J. Magn. Magn. Mater.*, 2008, **320**, 1106–1111.
- 52 C. Luo, W. Duan, X. Yin and J. Kong, *J. Phys. Chem. C*, 2016, **120**, 18721–18732.
- 53 W. Duan, X. Yin, C. Luo, J. Kong, F. Ye and H. Pan, *J. Eur. Ceram. Soc.*, 2017, **37**, 2021–2030.
- 54 Z. Ma, Q. Liu, J. Yuan, Z. Wang, C. Cao and J. Wang, *Phys. Status Solidi B*, 2012, **249**, 575–580.
- 55 Z. Guo, S. Park, H. T. Hahn, S. Wei, M. Moldovan, A. B. Karki and D. P. Young, *J. Appl. Phys.*, 2007, **101**, 09M511.
- 56 C. Liu, Y. Xu, L. Wu, Z. Jiang, B. Shen and Z. Wang, *J. Mater. Chem. A*, 2015, **3**, 10566–10572.
- 57 J. Li, H. Liu, J. Guo, Z. Hu, Z. Wang, B. Wang, L. Liu, Y. Huang and Z. Guo, *J. Mater. Chem. C*, 2017, **5**, 1095–1105.
- 58 V. Babrauskas and R. D. Peacock, *Fire Saf. J.*, 1992, **18**, 255–272.
- 59 X. Zhang, Q. He, H. Gu, H. A. Colorado, S. Wei and Z. Guo, *ACS Appl. Mater. Interfaces*, 2013, **5**, 898–910.
- 60 J. Gu, X. Meng, Y. Tang, Y. Li, Q. Zhuang and J. Kong, *Composites, Part A*, 2017, **92**, 27–32.
- 61 H. Chen and J. Kong, *Polym. Chem.*, 2016, **7**, 3643–3663.
- 62 W. Zhao, J. Kong, H. Liu, Q. Zhuang, J. Gu and Z. Guo, *Nanoscale*, 2016, **8**, 19984–19993.
- 63 D. Wang, K. Zhou, W. Yang, W. Xing, Y. Hu and X. Gong, *Ind. Eng. Chem. Res.*, 2013, **52**, 17882–17890.
- 64 J. W. Gilman, *Appl. Clay Sci.*, 1999, **15**, 31–49.
- 65 Y. L. Liu, *Polymer*, 2001, **42**, 3445–3454.
- 66 L. Chen, L. Song, P. Lv, G. Jie, Q. Tai, W. Xing and Y. Hu, *Prog. Org. Coat.*, 2011, **70**, 59–66.
- 67 H. Gu, X. Zhang, H. Wei, Y. Huang, S. Wei and Z. Guo, *Chem. Soc. Rev.*, 2013, **42**, 5907–5943.
- 68 K. Zhang, H.-O. Yu, Y.-D. Shi, Y.-F. Chen, J.-B. Zeng, J. Guo, B. Wang, Z. Guo and M. Wang, *J. Mater. Chem. C*, 2017, **5**, 2807–2817.
- 69 N. F. Colaneri and L. W. Schacklette, *IEEE Trans. Instrum. Meas.*, 1992, **41**, 291–297.
- 70 V. Babrauskas, R. H. Harris, R. G. Gann, B. C. Levin, B. T. Lee, R. D. Peacock, M. Paabo, W. Twilley, M. F. Yoklavich and H. M. Clark, *NBS Spec. Publ.*, 1988, **749**, 92.